NOAA Technical Report NESS 66

U.S. DEPARTMENT OF COMMERCE
National Oceanic and Atmospheric Administration
National Environmental Satellite Service

Effects of Aerosols on the Determination of the Temperature of the Earth's Surface From Radiance Measurements at 11.2 μm

H. JACOBOWITZ
K. L. COULSON

WASHINGTON, D.C.
September 1973

NOAA TECHNICAL REPORTS

National Environmental Satellite Service Series

The National Environmental Satellite Service (NESS) is responsible for the establishment and operation of the National Operational Meteorological Satellite System and of the environmental satellite systems of NOAA. The three principal offices of NESS are Operations, Systems Engineering, and Research. The NOAA Technical Report NESS series is used by these offices to facilitate early distribution of research results, data handling procedures, systems analyses, and other information of interest to NOAA organizations.

Publication of a report in NOAA Technical Report NESS series will not preclude later publication in an expanded or modified form in scientific journals. NESS series of NOAA Technical Reports is a continuation of, and retains the consecutive numbering sequence of, the former series, ESSA Technical Report National Environmental Satellite Center (NESC), and of the earlier series, Weather Bureau Meteorological Satellite Laboratory (MSL) Report. Reports 1 through 37 are listed in publication NESC 56 of this series.

Reports 1 through 50 in the series are available from the National Technical Information Service (NTIS), U.S. Department of Commerce, Sills Bldg., 5285 Port Royal Road, Springfield, Va. 22151. Price $3.00 paper copy; $1.45 microfiche. Order by accession number, when given, in parentheses. Beginning with 51, printed copies of the reports are available through the Superintendent of Documents, U.S. Government Printing Office, Washington, D.C. 20402. Price as indicated. Microfiche available from NTIS (use accession number when available). Price $1.45.

ESSA Technical Reports

NESC 38 Angular Distribution of Solar Radiation Reflected From Clouds as Determined From TIROS IV Radiometer Measurements. I. Ruff, R. Koffler, S. Fritz, J. S. Winston, and P. K. Rao, March 1967. (PB-174-729)

NESC 39 Motions in the Upper Troposphere as Revealed by Satellite Observed Cirrus Formations. H. McClure Johnson, October 1966. (PB-173-996)

NESC 40 Cloud Measurements Using Aircraft Time-Lapse Photography. Linwood F. Whitney, Jr., and E. Paul McClain, April 1967. (PB-174-728)

NESC 41 The SINAP Problem: Present Status and Future Prospects; Proceedings of a Conference Held at the National Environmental Satellite Center, Suitland, Maryland, January 18-20, 1967. E. Paul McClain, October 1967. (PB-176-570)

NESC 42 Operational Processing of Low Resolution Infrared (LRIR) Data From ESSA Satellites. Louis Rubin, February 1968. (PB-178-123)

NESC 43 Atlas of World Maps of Long-Wave Radiation and Albedo--for Seasons and Months Based on Measurements From TIROS IV and TIROS VII. J. S. Winston and V. Ray Taylor, September 1967. (PB-176-569)

NESC 44 Processing and Display Experiments Using Digitized ATS-1 Spin Scan Camera Data. M. B. Whitney, R. C. Doolittle, and B. Goddard, April 1968. (PB-178-424)

NESC 45 The Nature of Intermediate-Scale Cloud Spirals. Linwood F. Whitney, Jr., and Leroy D. Herman, May 1968. (AD-673-681)

NESC 46 Monthly and Seasonal Mean Global Charts of Brightness From ESSA 3 and ESSA 5 Digitized Pictures, February 1967-February 1968. V. Ray Taylor and Jay S. Winston, November 1968. (PB-180-717)

NESC 47 A Polynomial Representation of Carbon Dioxide and Water Vapor Transmission. William L. Smith, February 1969. (PB-183-296)

NESC 48 Statistical Estimation of the Atmosphere's Geopotential Height Distribution From Satellite Radiation Measurements. William L. Smith, February 1969. (PB-183-297)

NESC 49 Synoptic/Dynamic Diagnosis of a Developing Low-Level Cyclone and Its Satellite-Viewed Cloud Patterns. Harold J. Brodrick and E. Paul McClain, May 1969. (PB-184-612)

NESC 50 Estimating Maximum Wind Speed of Tropical Storms From High Resolution Infrared Data. L. F. Hubert, A. Timchalk, and S. Fritz, May 1969. (PB-184-611)

(Continued on inside back cover)

U.S. DEPARTMENT OF COMMERCE
Frederick B. Dent, Secretary

NATIONAL OCEANIC AND ATMOSPHERIC ADMINISTRATION
Robert M. White, Administrator

NATIONAL ENVIRONMENTAL SATELLITE SERVICE
David S. Johnson, Director

NOAA Technical Report NESS 66

Effects of Aerosols on the Determination of the Temperature of the Earth's Surface From Radiance Measurements at 11.2 μm

H. Jacobowitz
K. L. Coulson

WASHINGTON, D.C.
September 1973

UDC 551.521.2:551.510.42

551.5 Meteorology
.510 Atmospheric structure and composition
.42 Impurities and dust
.521 Radiation
.2 Terrestrial radiation

For sale by the Superintendent of Documents, U.S. Government Printing Office, Washington, D.C., 20402.
Price $0.55

U. S. DEPARTMENT OF COMMERCE
National Oceanic and Atmospheric Administration
National Environmental Satellite Service

Washington, D. C.
19 November 1973

- ERRATA -

EFFECTS OF AEROSOLS ON THE DETERMINATION OF THE TEMPERATURE OF THE EARTH'S SURFACE FROM RADIANCE MEASUREMENTS AT 11.2 μm

by H. Jacobowitz
and
K. L. Coulson

NOAA TECHNICAL REPORT NESS 66

September 1973

Page 2:

Line 19 - Mariatt should read Marlatt

Page 7:

Line 3 - $t_{\lambda}(Z,h)$ should read $\tau_{\lambda}(Z,h)$

Page 8:

Line 15 - 0.8 should read 0.08

Page 11:

Line 6 - ν 3.5, 4.0, and 5.0 should read ν = 3.5, 4.0, and 5.0

Page 14:

Line 13 - T should read ΔT

CONTENTS

EFFECTS OF AEROSOLS ON THE DETERMINATION OF THE TEMPERATURE OF THE EARTH'S SURFACE FROM RADIANCE MEASUREMENTS AT 11.2 μm

H. Jacobowitz

National Environmental Satellite Service
Washington, D. C.

and

K. L. Coulson

University of California
Davis, California

ABSTRACT. The influence of atmospheric aerosols on outgoing terrestrial radiation in the window region at 11.2 μm is estimated by atmospheric modeling. Nine different particle size distributions, 3 vertical aerosol concentration profiles, and 5 vertical temperature profiles are considered, for a total of 135 atmospheric models. For each model, the upward radiant intensity was computed for every 0.2 km from the surface to 20 km. From these values, equivalent black-body temperatures were determined as a function of height, and the error in the derived surface temperature due to aerosols was computed. Results show that absorption by aerosols is dominant over emission, making the deduced surface temperature lower than actual, except in the subarctic winter. Errors were generally less than 2°K except under extreme conditions.

I. INTRODUCTION

The influence that aerosols (atmospheric particulate matter) have on the radiation emitted to space from the earth-atmosphere system has come under increasing study in the past few years, particularly with regard to the climatic changes that may be taking place as a result of the increase in the pollution levels in our atmosphere. While such studies are of great value, the radiative studies are also important in assessing the effects of aerosols on the radiometric measurements made routinely from earth-orbiting satellites.

For example, vertical temperature profiles are deduced from radiometric measurements made in several narrow spectral intervals in one or more atmospheric absorption bands. However, these deductions require an accurate knowledge of the transmission properties of the atmosphere in those bands. While the transmission trhough the principal atmospheric gases is accounted for, the transmission through the aerosols is generally neglected. It is therefore of interest to study how this neglect affects temperature determinations and to learn how one can compensate for aerosol effects.

It was for these purposes that the present study was initiated. Although emphasis will be on possible errors that may be produced in the surface temperature by a neglect of the effects of aerosols, the results will be

applicable to certain other problems as well.

Recently, Stowe (1971) investigated absorption and scattering by aerosols of radiation in the various spectral regions currently used for atmospheric sounding. It was found that the intensity of the radiation scattered by the aerosols is small compared to that emitted. Thus we assume that accuracy will still be sufficient if scattering is neglected. Stowe used the "Haze M" particle size distribution of Deirmendjian (1969) and the vertical profiles of particle concentration obtained by Rosen (1967) and Elterman (1968). He estimated that radiance determinations may be in error by as much as 15% in the most transparent part (13.33 μm) of the 15 μm band of carbon dioxide because of a neglect of absorption by aerosols. He also found that most of the radiation absorbed from the upward stream is compensated for by radiation emitted from the aerosol particles themselves, thereby reducing errors in radiance estimates to generally less than 1%. According to Stowe's analysis, errors in the remote sensing of the temperature profiles are due to (1) large underestimates of the atmospheric emission and (2) errors in the weighting functions used for inverting the radiometric measurements caused by a neglect of the effects of atmospheric aerosols.

In a recent study of aerosol effects in the natural atmosphere Marlatt et al. (1971) measured atmospheric aerosol size distribution and sea surface temperatures from altitudes ranging from 400 to 37,300 feet. Using the measured aerosol concentrations and nearby radiosonde temperatures, he was able to determine that for very hazy conditions with cloudless skies, error in the computed blackbody temperature in the 8- to 14 μm window region due to neglect of the observed aerosol absorption was of the order 1°K.

For the present study we have focused our attention on estimating theoretically the effect of aerosols on the 11-μm window region. This region was chosen to minimize the perturbing effects of absorption by atmospheric gases and to estimate what accuracy of surface temperature determinations can be reasonably expected from satellite measurements. The analysis can be readily generalized to include other spectral regions.

2. ATMOSPHERIC MODELS

Calculations were made for a variety of model atmospheres. Since we were chiefly interested in computing the difference in upward intensities when aerosols were included and when aerosols were excluded, it was assumed that the gaseous component of the atmosphere could be omitted from the models without introducing serious errors. This is equivalent to the assumption that the effect of the gases upon the emitted radiation is independent of the effect of the aerosols, i.e., their combined effects are additive. Although this is probably a poor assumption for many atmospheric absorption bands, it should be a good one for the window region because of the weak molecular absorption in that region.

Natural aerosols generally range in radius from 0.001 to 100 μm although the greatest concentrations of the particles are generally between 0.1 and 10 μm. When there are dust storms, fog, or smog, the distribution is changed somewhat by the addition of particles generally exceeding 1 μm in

size. Junge (1953) found that the observed size distribution could be described reasonably well by the expression

$$\frac{dN}{dr} = C\, r^{-4}, \qquad (1)$$

where N is the particle concentration, r is the particle radius, and C is a proportionality constant. Later investigations by Junge (1955) showed that (1) could be generalized as

$$\frac{dN}{dr} = C\, r^{-\nu}, \qquad (2)$$

where ν, generally known as the Junge distribution parameter, is only approximately equal to 4. Variations of ν from 4 occur as a result of humidity changes, dust storms, or other variations in atmospheric phenomena.

To explore the influence of the particle size distributions on the radiation transferred by the atmosphere, three values of ν (3.5, 4.0, and 5.0) and three size ranges (0.08 to 10.0 μm, 0.06 to 5.0 μm, and 0.04 to 3.0 μm) were chosen since their scattering and extinction cross sections were available (I. L. Zel'manovich and K. C. Shifrin, 1971).

To distinguish among clear, hazy, and very hazy atmospheres, vertical profiles of aerosol number density based upon those of McClatchey et al. (1971) were used. These are shown in figure 1, where the upper limit chosen is an altitude of 20 km. The aerosol concentration above this level in their

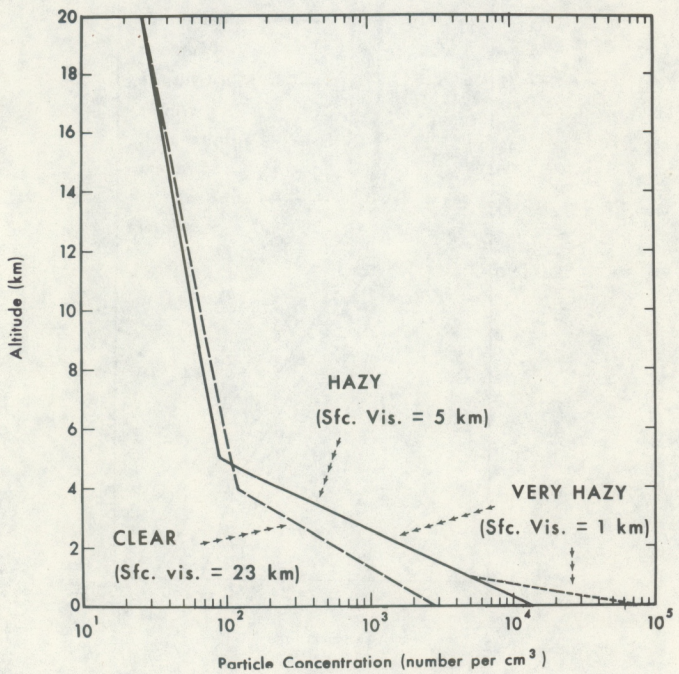

Figure 1.--Vertical profiles of aerosol particle concentration for clear, hazy, and very hazy atmospheric conditions.

models is too low to have any significant effect upon the radiation field. For the clear and hazy atmospheres, the number density at the surface is such that the surface visibilities for the case that $0.08 \leq r \leq 10.0$ μm and $\nu = 4.0$ are 3 and 5 km, respectively. A model of a very hazy atmosphere was constructed from that of the hazy atmosphere by arbitrarily extrapolating the concentration of the hazy atmosphere at the 1-km level to a surface value corresponding to a visibility of 1-km.

The models used for the aerosol distributions then were specified completely by assuming that the relative size distributions were independent of altitude. Bu combining the 9 relative size distributions with the 3 vertical concentration profiles, we obtained 27 models of the aerosol distribution.

All that remains to be specified in the atmospheric models are the vertical temperature profiles. Again, following McClatchey et al, (1971), we chose 5 profiles corresponding to mean conditions in the tropics and to the summer and winter seasons for the midlatitudes and subarctic regions (fig. 2). Each of the 5 temperature profiles were combined with each of the 27 aerosol profiles to make a total of 135 model atmospheres for which computations were made.

3. RADIATIVE COMPUTATIONS

The scattering and extinction cross sections of the aerosols tabulated by Zel'manovich and Shifrin were computed using the complex index of refraction corresponding to that for water at a temperature of 20°C. The extinction and scattering properties for the different aerosol models at a wavelength

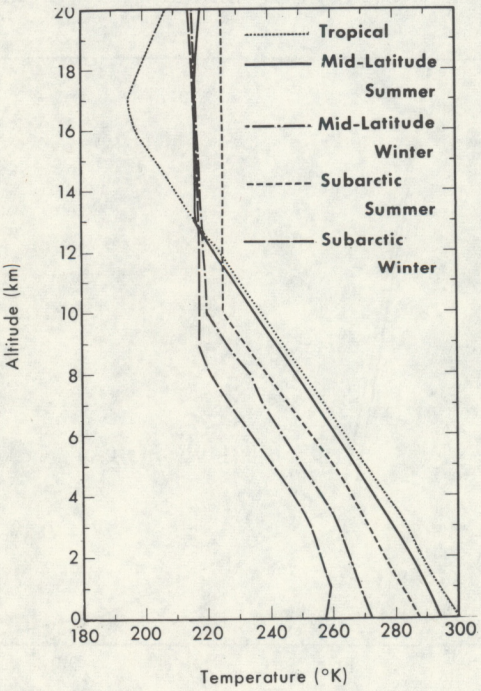

Figure 2.--Vertical profiles of the mean temperature for the tropical region and for the summer and winter seasons of the midlatitude and subarctic regions.

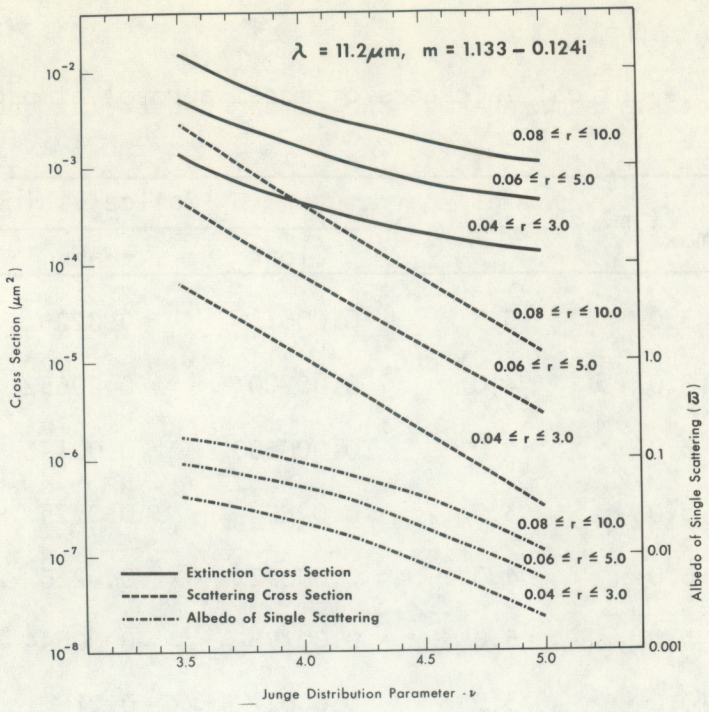

Figure 3.--Extinction and scattering cross sections and the albedo of single scattering vs. the Junge distribution parameter (ν) for the wavelength (λ) and index of refraction (m) indicated. Size ranges of the particles are given to the right of each curve.

equal to 11.2 μm can be seen from the plot of effective cross section (extinction: σ_{ext}; scattering; σ_{ext}) vs. the Junge exponent ν (fig. 3). The results have been normalized by dividing the effective cross section for the aerosols by the total number of particles assumed, which yields an effective cross section of one particle which is radiatively typical of the total aerosol model.

One of the basic parameters that characterize the transfer of radiation by the aerosols is the extinction optical thickness τ_λ of a layer. This is defined to be the property of a layer that causes unit radiation of wavelength λ normally incident upon it to be reduced to $e^{-\tau_\lambda}$ in passing through the layer. It may be computed from a knowledge of the extinction cross section of the aerosols and their vertical concentration profile by means of the equation

$$\tau_\lambda(h) = \sigma_{\lambda,ext} \int_0^h N(Z)dZ \,, \qquad (3)$$

where $\sigma_{\lambda ext}$ is the normalized extinction cross section at the wavelength λ for a unit aerosol concentration, N(Z) is the concentration as a function of the altitude Z and h is the altitude of the top of the aerosol layer. The cross sections given by Zel'manovich and Shifrin and the vertical concentration profiles shown in fig. 1 were used in eq. (3) to compute the optical thickness as a function of the altitude for all 27 aerosol models. Table I

TABLE I.--Optical thickness of model aerosol atmospheres

r_{min} (m)	r_{max} (m)	ν	Optical thickness		
			Clear	Hazy	Very hazy
.04	3.0	3.5	0.00613	0.0200	0.01418
.04	3.0	4.0	0.00200	0.00652	0.0136
.04	3.0	5.0	0.000600	0.00196	0.00409
.06	5.0	3.5	0.0222	0.0725	0.152
.06	5.0	4.0	0.00692	0.0226	0.0472
.06	5.0	5.0	0.00198	0.00644	0.0135
.08	10.0	3.5	0.0662	0.216	0.451
.08	10.0	4.0	0.0182	0.0593	0.124
.08	10.0	5.0	0.00468	0.0152	0.0319

shows the resulting optical thickness for the models for the layer extending from the surface to the 20-km level.

From the variation of the optical thickness with altitude, the transmissivity from any level in the model to any other level could be readily computed. By restricting the study to a narrow spectral interval and assuming that scattering is small compared to absorption (a reasonable assumption for most of the aerosol models) one can approximate the transmissivity in the vertical from the altitude Z_1 to the altitude Z_2 by the expression

$$\tau_\lambda(Z_1,Z_2) = e^{-\left\{t_\lambda(Z_2) - t_\lambda(Z_1)\right\}\sec\theta} \tag{4}$$

where $\tau_\lambda(Z_1,Z_2)$ is the transmissivity, $t_\lambda(Z_1)$ and $t_\lambda(Z_2)$ are the optical thicknesses from the surface to the levels Z_1 and Z_2, respectively, and θ is the angle between the direction of the radiation and the vertical. For the present study, the radiation was considered only in the vertical direction, in which case sec θ = 1.0.

The intensity of radiation at any altitude h may be computed from the relation

$$I_\lambda^{\uparrow}(h) = \varepsilon_\lambda B_\lambda(T_o)\tau_\lambda(0,h) + \int_o^h B_\lambda\left(T(Z)\right)\frac{d\tau_\lambda(Z,h)}{dZ}\,dZ \tag{5}$$

where $I_\lambda^\uparrow(h)$ is the intensity of the upward radiance at the altitude h, $B_\lambda(T)$ is the blackbody radiance at the temperature T, T_o is the surface temperature, $\tau_\lambda(Z,h)$ is the transmissivity from the altitude Z to the altitude h, ε_λ is the surface emissivity, and λ is wavelength. Since the temperature and transmissivity are given at a finite number of levels, (5) was replaced by the approximate expression;

$$I_\lambda^\uparrow(Z_\ell) \approx B_\lambda(T_o)\tau_\lambda(0,Z_\ell) + \sum_{m=0}^{\ell-1} \left\{ \frac{B_\lambda\left(T(Z_m)\right) + B_\lambda\left(T(Z_{m+1})\right)}{2} \right\} \{\tau_\lambda(Z_{m+1},Z_\ell) - \tau_\lambda(Z_m,Z_\ell)\} \tag{6}$$

where Z represents the altitude of the ℓ_{th} level and ε_λ has been set to unity for all model atmospheres.

The equivalent blackbody temperature, T_{eq}, that corresponds to the radiant intensity $I_\lambda^\uparrow(Z_\ell)$ is defined by the expression,

$$B_\lambda(T_{eq}) = I_\lambda^\uparrow(Z_\ell) \ . \tag{7}$$

Comparing this with the surface temperature T_o, the temperature error ΔT is defined by the relation

$$\Delta T = T_o - T_{eq} \ . \tag{8}$$

This quantity, which is of primary interest in the study, represents the error in the determination of the temperature from a measurement of the radiance at some altitude above the surface. In the absence of any aerosol or molecular components to the atmosphere, $T_{eq} = T_o$ and therefore $\Delta T = 0$. With aerosols and air molecules in the atmosphere, $T_{eq} \neq T_o$, due to the absorption and emission that takes place in the atmosphere.

The transport of radiation through the model atmospheres was computed and analyzed by means of eqs. (4) to (8). The procedure used was:

(1) Compute the optical thickness as a function of altitude for every 0.2 km from the surface to an altitude of 20 km for each of the 27 aerosol models using (3).

(2) Determine the transmissivities between each of the levels for each aerosol model using (4).

(3) Compute the intensity of radiation directed vertically upward at each level for each aerosol model and for each of the 5 temperature profiles (135 model atmospheres) using (6).

(4) Calculate the equivalent blackbody temperature T_{eq} from the upward radiation intensity values by means of (7).

(5) Determine the temperature errors by (8), using T_{eq} as determined from the radiance values and T_o as assumed in the atmospheric models.

4. RESULTS OF THE CALCULATIONS

A. Extinction and Scattering by Aerosols

The general extinction and scattering characteristics of the different aerosol models can be seen in the curves of effective cross section (fig. 3). The effective cross section corresponds to that for a single effective particle representative of each distribution.

The curves for the extinction cross section σ_{ext} show there is a relatively strong dependence of extinction cross section on the range of the radii taken into account. For instance, σ_{ext} for $0.08 \leq r \leq 10.0$ μm is about an order of magnitude greater than that for $0.04 \leq r \leq 3.0$ μm, and the ratio between these extinction cross sections is practically independent of ν. Physically, an increase of the minimum size from 0.04 to 0.08 μm effectively eliminates many small particles from consideration, since the Junge distribution contains many small particles. Conversely, an increase of the upper size limit does not add many particles, but those added are very effective attenuators. The net result, as the size limits for the radii increase, is an increase in the size of the average particle of the distribution and an increase in the value of the extinction cross section.

The same reasonsing can be applied to the curves of the scattering cross section, σ_{scat}. However, for a given value of ν, the rate of increase of σ_{scat} with increase in the limits of the radii is greater than that for σ_{ext}. This can be explained with the aid of figure 4 in which the extinction and scattering efficiency factors ($Q_{ext} = \sigma_{ext}/\pi r^2$ and $Q_{scat} = \sigma_{ext}/\pi r^2$) are plotted versus the particle radius r for three different values of the complex index of refraction ($Q_{ext} > Q_{scat}$). While the real part of the index of refraction is the same for all three cases, the imaginary part differs. The index for the middle curve of each set is the same as that used in obtaining the results of figure 3. By comparing the curves in figure 4 with the superimposed straight lines that have geometric slopes equal to 1 and 4, it can be concluded that $\sigma_{scat}/\pi r^2 \sim r^4$ and $\sigma_{ext}/\pi r^2 \sim r$ for all but the largest values of the particle radius. Then, $\sigma_{scat} \sim r^6$ and $\sigma_{ext} \sim r^3$ for sufficiently small values of r. The scattering cross section, therefore, is particularly sensitive to the sizes of the scattering particles, and anything that changes the average size of the distribution has more effect on σ_{scat} than on σ_{ext}. This property is responsible for the large spread of the curves of figure 3 for the three size ranges.

The dependence of the scattering and extinction cross sections on the radius also explains the decrease in the value of the cross sections with increase in the Junge exponent ν. By increasing the magnitude of ν, a steeper negative slope is given to the distribution. This increases the number of small particles at the expense of the large ones and therefore decreases the size of the average particle causing the cross sections to decrease. Again, because of the greater sensitivity of σ_{scat} to particle size than σ_{ext}, the curves for

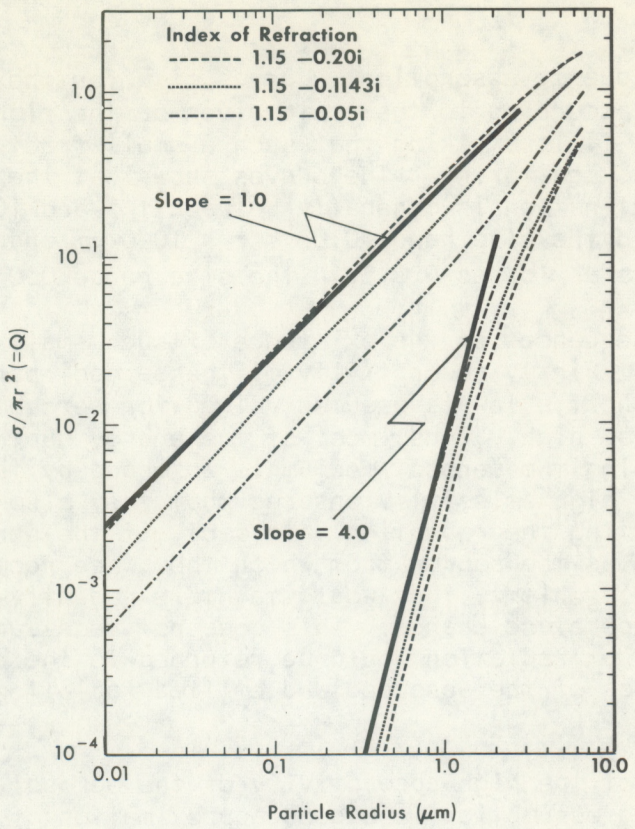

Figure 4.--Extinction and scattering efficiency factors $Q(=\sigma/\pi r^2)$ versus the radius r for the wavelength λ and index of refraction (m) Solid lines that have geometric slopes of 1 and 4 are superimposed for the purpose of comparison.

σ_{scat} decrease more rapidly with increasing ν than the curves for σ_{ext}. For instance, in figure 3 the curve for the middle size range shows a decrease in σ_{scat} by a factor of 180 from ν = 3.5 to ν = 5.0, but a decrease of only 12.5 for σ_{ext}.

Since the total attenuation is produced by a combination of absorption and scattering, we can write for the respective cross sections the relation

$$\sigma_{ext} = \sigma_{abs} + \sigma_{scat} \tag{9}$$

By dividing by σ_{ext} we obtain the quantity

$$\frac{\sigma_{scat}}{\sigma_{ext}} = 1 - \frac{\sigma_{abs}}{\sigma_{ext}} \tag{10}$$

which is designated the albedo of single scattering, $\bar{\omega}$. Physically, it represents the part of the total attenuation that is contributed by scattering. Then the quantity

$$1 - \bar{\omega} = \frac{\sigma_{abs}}{\sigma_{ext}} \tag{11}$$

represents the part due to absorption. Curves of $\bar{\omega}$ for the various aerosol models are plotted, according to the scale given on the right, as the bottom family in figure 3. It is striking that such a small fraction of the total attenuation is due to scattering. The curves show that the contribution of scattering to the extinction is generally between 1 % and 10 % of the total. Only for particles in the size range $0.08 \leq r \leq 10.0$ μm and $\nu = 4.0$ is $\bar{\omega} > 10$ %, and it gets as low as 0.2 % in the size range $0.04 \leq r \leq 3.0$ μm.

There are two consequences of the existence of such small values of $\bar{\omega}$ for the present problem. First, absorptivity of the aerosol particles is high, which means if Kirchhoff;s law is assumed valued for aerosols, that their emissivity is likewise high. Thus, most of the energy subtracted from a beam of radiation traversing the aerosol medium is absorbed by the aerosol particles, but their high emissivity ensures that they also lose energy efficiently by remitting the radiation. In fact, if the particles were at the same temperature as the source from which they were receiving radiation (the surface in this problem), they would maintain radiative equilibrium and would undergo no temperature change. This does not necessarily mean, however, that the same amount of radiation would be returned to the original beam, as the angular dependence of the absorbed and emitted radiation may not be the same.

The second result of the high absorptivity of the aerosol particles is that the single scattering assumption is a good approximation of reality. Because of single scattering the radiative field is weak; the series attributable to secondary and higher order scattering of already scattered radiation converges rapidly. If 10 % is due to primary scattering, only 1 % would be due to secondary scattering, 0.10 % to tertiary scattering, etc. Thus, any errors caused by neglect of multiple scattering would be minor compared to those of the unknown physical validity of the models.

The relatively strong decrease of $\bar{\omega}$ with increasing ν and the close spacing of the three curves of $\bar{\omega}$ shown in figure 3 both indicate the high absorptivity of small particles in comparison with that of large particles. As pointed out above, $\sigma_{scat} \sim r^6$ and $\sigma_{ext} \sim r^3$ for small particles. Since σ_{ext} is dominated by σ_{abs}, one can also write $\sigma_{abs} \sim r^3$. Thus, as particle size decreases, σ_{scat} decreases about 10^3 times as fast as σ_{abs}, thus producing the result shown.

B. Aerosol Effects on Temperature Determinations

Using the atmospheric models discussed above, computations have been made for determining the error that would be produced by various aerosol distributions in the intervening atmosphere in surface temperature determinations from satellite altitude. The temperature error ΔT is defined here as the difference between the actual temperature, i.e., that assumed to exist at the surface, and the equivalent blackbody temperature which would be deduced from measurements of the upward radiance at the top of the atmosphere. Thus a positive value of ΔT indicates the actual temperature exceeds that measured, and vice versa.

The temperature errors determined by this procedure are plotted as a function

of the Junge distribution parameter ν for the five models of atmospheric temperature profile in figures 5 to 9. In each case, computations of ΔT have been made for three different intervals of particle size and for clear, hazy, and very hazy atmospheric conditions.

Results for the tropical atmosphere are shown in figure 5. The curves are defined by three points each, the points corresponding to ν=3.5, 4.0, and 5.0. As would be expected from the results shown previosuly in figure 3, the largest temperature errors are for the largest aerosol size range ($0.08 \leq r \leq 10.0$ µm), for $\nu = 3.0$, and for the very hazy atmosphere. For this worst case ΔT approaches 2.0°K.

Just how realistic this worst case is for actual atmospheric conditions is hard to say. We do not know enough about the aerosols that exist in the atmosphere, particularly in the tropical atmosphere, to make a firm judgment. However, the very hazy atmospheric model, with its low horizontal visibility, does not occur freq uently in the tropics. The clear model is probably more applicable for tropical atmospheres, and ΔT for the worst clear case is only about 1°K. If the Junge distribution parameter ν has a more moderate value of 4.0, as has been found to be the case in many instances, then ΔT for the clear tropical atmosphere is only about 0.25°K.

Throughout the computations, it is shown that ΔT is very sensitive to the range of particle sizes assumed. The magnitude of ΔT decreases by a factor of about 10 as the size range assumed decreases from $0.08 \leq r \leq 10.0$ µm to $0.04 \leq r \leq 3.0$ µm. This means that the error comes within the noise of measurements for the smaller size range, but that the result of aerosols of

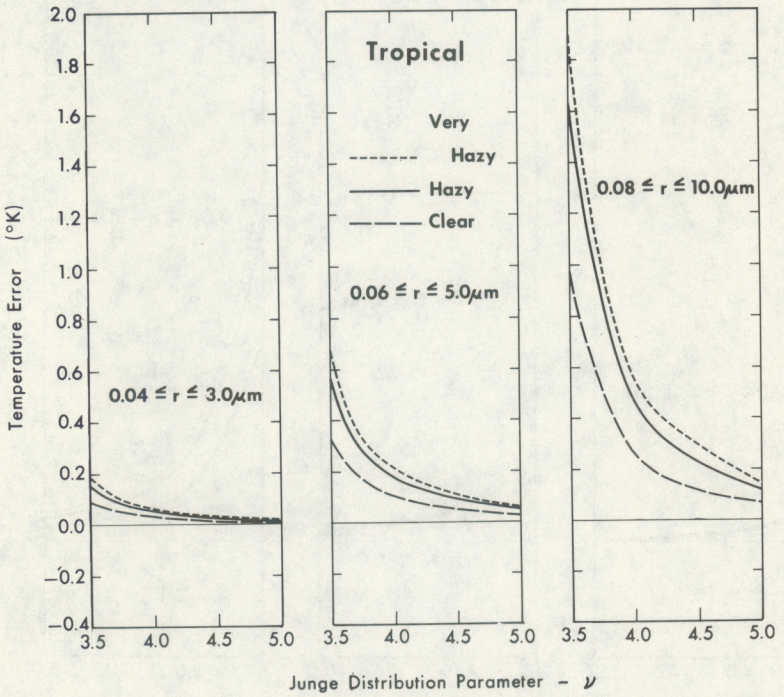

Figure 5.--Temperature error ΔT versus the Junge distribution parameter ν for a tropical atmosphere for three degrees of haziness and the particle size ranges indicated. The wavelength is 11.2 µm.

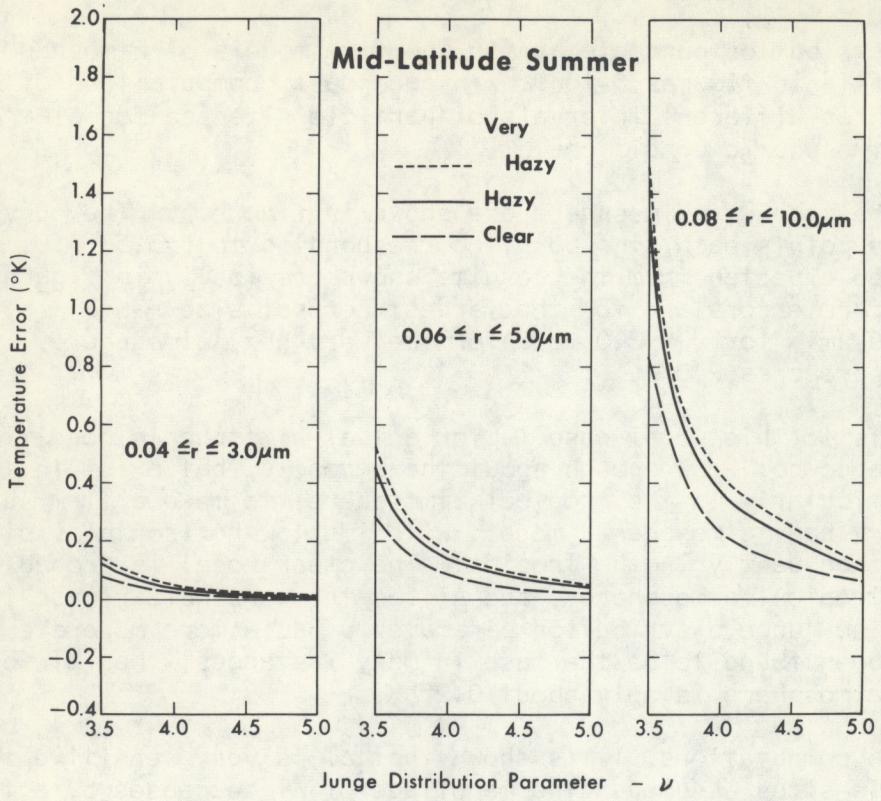

Figure 6.--Same as figure 5, mid-latitude summer.

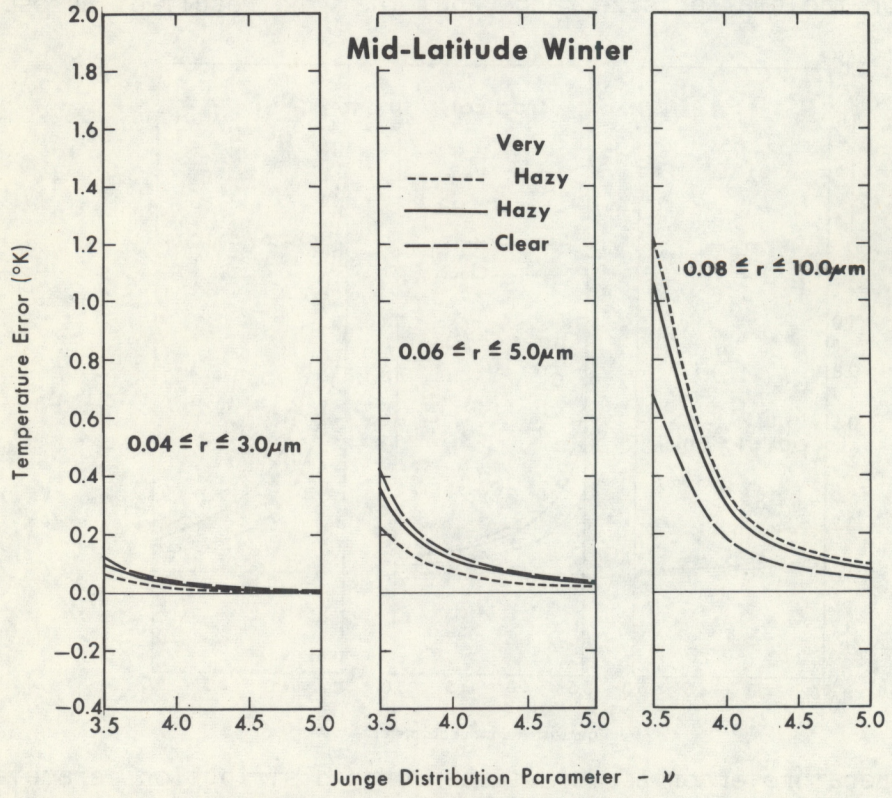

Figure 7.--Same as figure 5, mid-latitude winter.

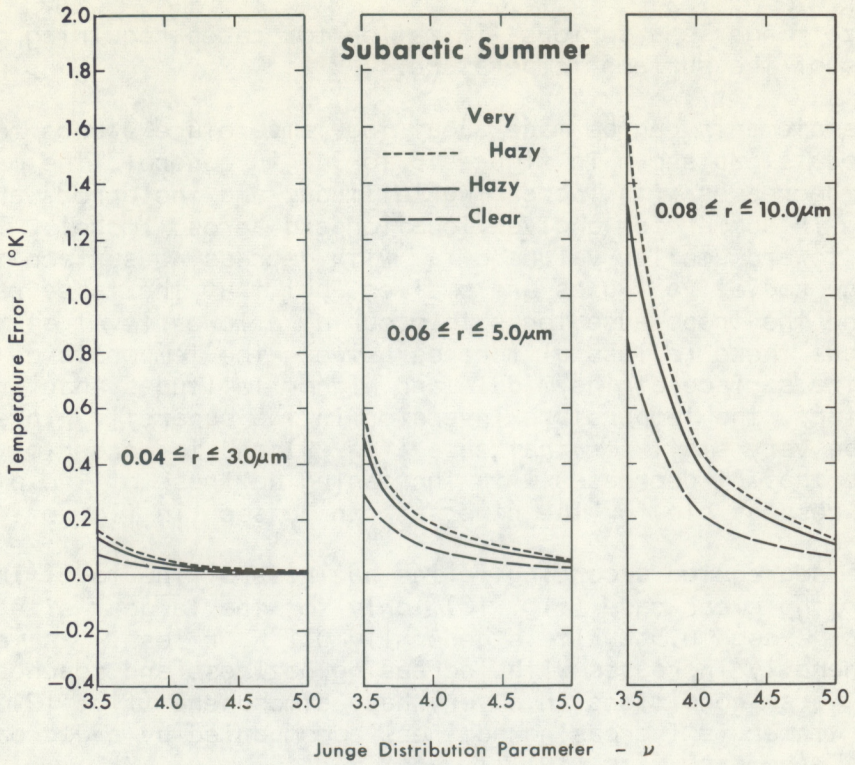

Figure 8.--Same as figure 5, subarctic summer.

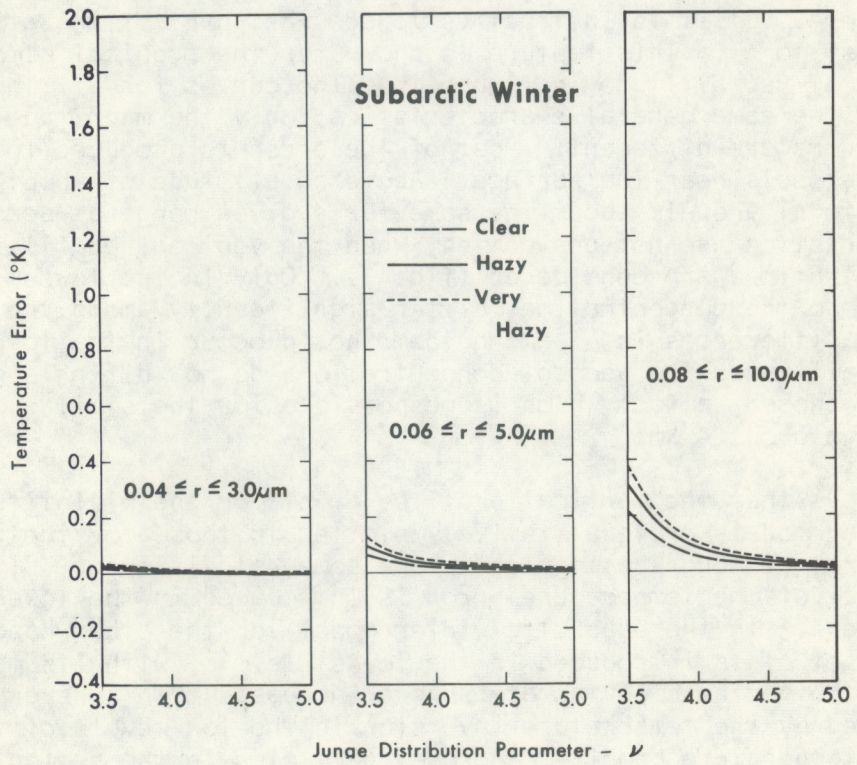

Figure 9.--Same as figure 5, subarctic winter.

the larger size range is a serious limitation for cases requiring precise determinations of the surface temperature.

Comparable statements can be made about the temperature errors for other atmospheric models, as shown in figures 6 to 9. In general, the magnitude of the errors decreases with increasing latitude, and the errors are smaller in winter than in summer for a given location and aerosol model. The reason for the trend toward smaller values of ΔT with decreasing surface temperature is not that the radiative fluxes are smaller, but that the lapse rates are more stable and the tropopause tends to occur at a lower level at the higher latitudes. Thus there is less difference between the temperatures of the aerosols and the surface at the middle and higher latitudes than in the tropics. In fact, the temperature inversion in the subarctic winter model causes ΔT to be very small for that case (fig. 9) and the order of the curves is reversed so that ΔT decreases with increasing haziness of the atmosphere. The mechanism responsible for the reversal can be seen in figure 14.

The data are segregated according to the haziness of the model in figures 10 to 12. For the clear case (fig. 10), only for the largest size range and $\nu < 4.0$ does ΔT exceed 0.5°K, it is generally 0.2°K or less. As mentioned before, ΔT generally increases with increasing haziness and reaches nearly 2.0°K for the worst conditions in a very hazy atmosphere (fig. 12). Only for the subarctic winter is increasing haziness accompanied by a decreasing magnitude of ΔT (compare figs. 10, 11, and 12).

The results so far have been for radiation emerging to space from the top of the atmosphere, but it is instructive to see what part of the atmosphere contributes most to ΔT. This feature is shown for the tropical atmosphere by the plot of ΔT vs. altitude in figure 13. The curves for all three size ranges exhibit the same general characteristics; only the magnitude of the temperature errors are different. Most of the error is produced in the highly concentrated aerosols near the surface. Above an altitude of about 4 km, the contributions to ΔT are all about the same for a given range of aerosol sizes. These characteristics are not unexpected, when the vertical profiles of aerosol concentrations are considered (fig. 1). Only in the lowest levels of the atmosphere do the concentrations differ significantly among the models, so the primary differences in ΔT among them should occur in the lowest levels. At the higher altitudes the aerosol concentrations do not differ significantly for the models chosen, a fact which is responsible for the similar slopes of the curves above about 4 km.

Figure 14 shows that the vertical profiles of ΔT for the midlatitude and subarctic summer models are qualitatively similar to those for the tropical model atmosphere, although the magnitudes are somewhat different. In all of these cases most of the temperature error is introduced in the lowest layers of the atmosphere. In the subarctic winter model, on the other hand, a small negative value of ΔT is introduced in the lowest levels, with its magnitude increasing as the haziness of the atmosphere increases. This reversal of sign is produced by the temperature inversion in the low levels of the subarctic winter temperature profile. Aerosol particles in the region from the surface to about 2 km altitude are at a temperature higher than that of the surface, and as a consequence add more radiation into the upward stream by emission than they subtract by absorption. Above the inversion, a greater

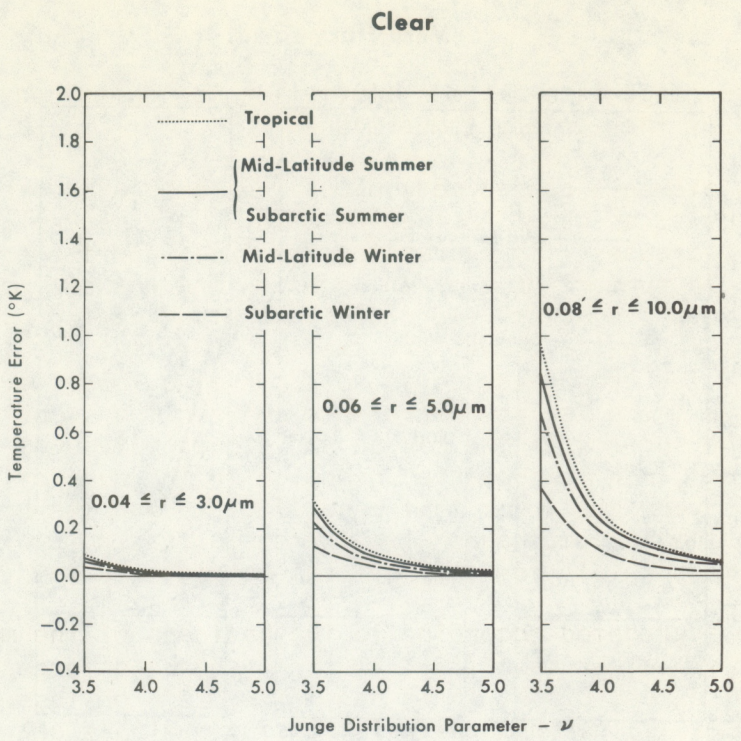

Figure 10.--Temperature error ΔT vs, the Junge distribution parameter ν for a clear atmosphere for five atmospheric temperature profiles and the particle size ranges indicated. The wavelength is 11.2 μm.

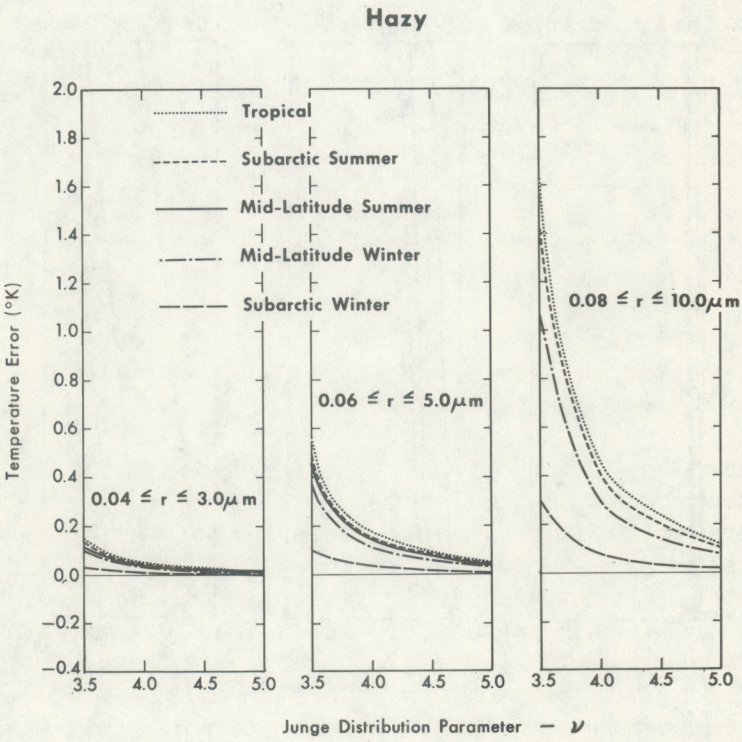

Figure 11.--Same as figure 10, hazy atmospnere.

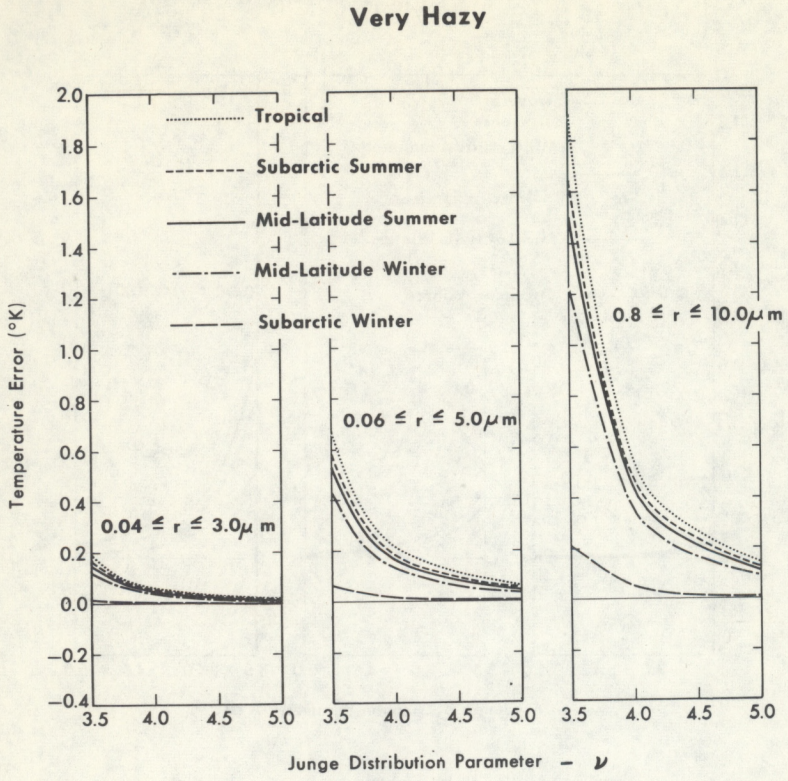

Figure 12.--Same as figure 10, very hazy atmosphere.

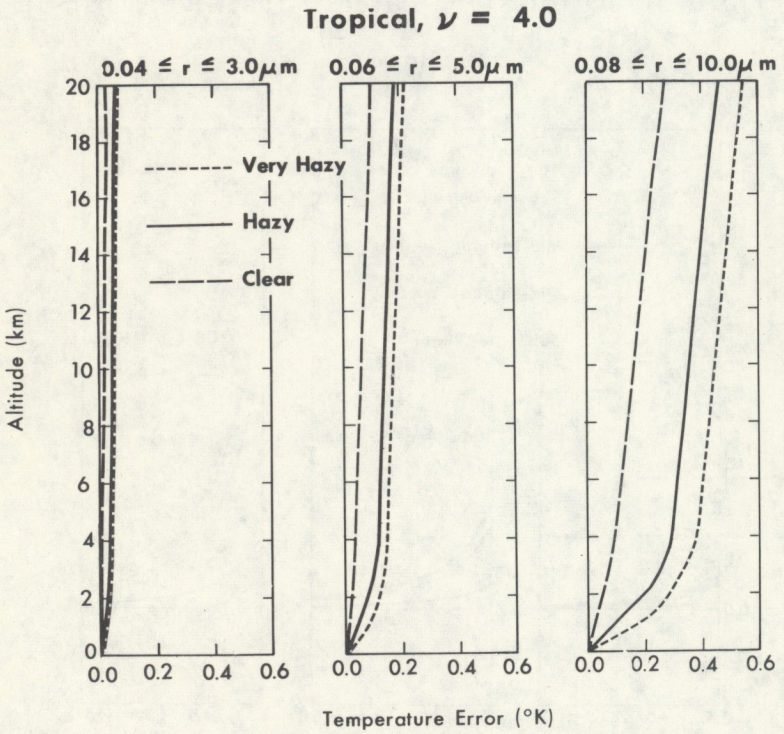

Figure 13.--Temperature error ΔT vs. altitude for a tropical atmosphere for three degress of haziness, a single value of the distribution parameter ν, and particle size ranges indicates. The wavelength is 11.2 μm.

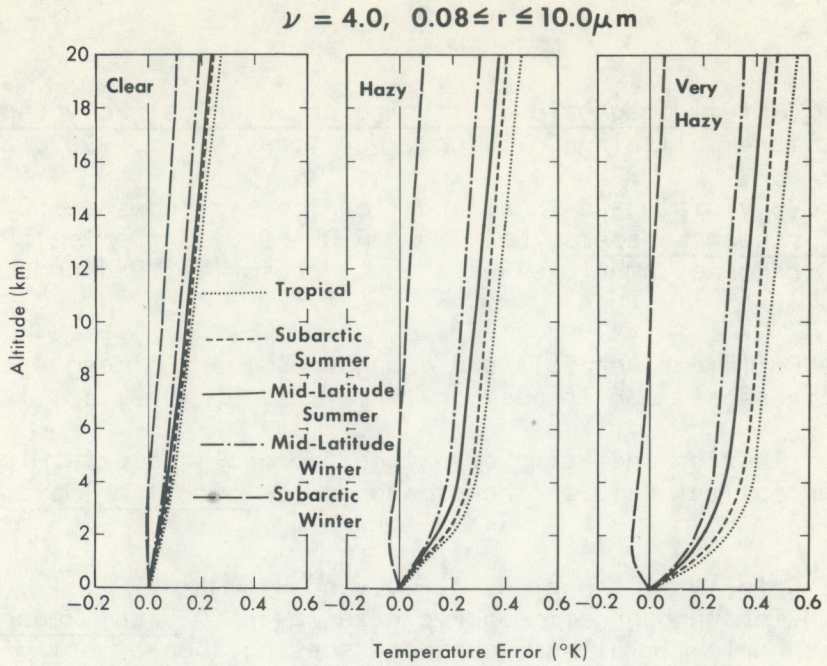

Figure 14.--Temperature error ΔT vs. altitude for the size range .08 < r < 10.0 μm and the Junge distribution parameter ν = 4.0 for 3 degreees of haziness and 5 temperature profiles indicated.

absorption than emission of energy by the particles causes the curves for the subarctic winter model to assume the same general character as that of the other models, but the negative values have to be compensated for by colder layers before the errors become positive. This results both in very small final errors of ΔT for the subarctic winter atmosphere, and in a decrease of error with increasing haziness in contrast to the other cases. By a small increase of the temperature inversion in the model, the temperature error could be completely erased or reversed in sign for the subarctic winter atmosphere. Such an inversion is not at all unusual in subarctic or arctic regions, although it apparently does not occur as a mean condition.

ACKNOWLEDGEMENTS

The figures were drafted by Robert Ryan, the manuscript was typed by Betty Loveless, and Paul Pellegrino computed and graphed most of the results.

REFERENCES

Deirmendjian, D., Electromagnetic Scattering on Spherical Polydispersions, American Elsevier Publishing Co., Inc., New York, N. Y., 1969, 290 pp.

Elterman, L., "UV, visible and IR attenuation for altitudes to 50 km," Environmental research papers, No. 285, AFCRL-68-0153, Optical Physics Laboratory, Air Force Cambridge Research Laboratories, Bedford, Mass., 1968, 49 pp.

Junge, C., "Die Rolle der Aerosole und der gasförmigen Beimengungen der Luft im Spurenstoffhaushalt der Troposphäre," Tellus, 5, 1953, pp. 1-26.

"The size distribution and aging of natural aerosols as determined from electrical and optical data on the atmosphere," Journal of Meteorology, 12, 1955, pp. 13-25.

Marlatt, W. E., Cole, H. I., Harlan, J. C., and Hjermstad, J. I., "Infrared radiation transfer through atmospheric haze layers," Final Report, NAS 5-11631, Atmospheric limiations to remote sensing, Department of Watershed Science, Colorado State University, Fort Collins, Colo., 1971, 62 pp.

McClatchey, R. A., Fenn, R. W., Selby, J. E. A., Volz, F. E., and Garing, J. S., "Optical properties of the atmosphere (revised)". Environmental research papers, No. 354, AFCRL-71-0279, Optical Physics Laboratory, Air Force Cambridge Research Laboratories, Bedford, Mass., 1971, 85 pp.

Rosen, James M., "Simultaneous dust and ozone soundings over North and Central America", University of Minnesota-Atmospheric Physics-25, Report #N68-11414, 1967.

Stowe, Larry L., Jr., "The effects of particulate matter on the radiance of terrestrial infrared radiation", Institute of Geophysics and Planetary Physics, University of California, Los Angeles, 1971, 109 pp.

Zel'manovich, I. S. and Shifrin, K. C., Tables of Light Scattering, Vol. IV, Leningrad, U.S.S.R., Hydrometeorological Office, 1971, 167 pp.

☆ U.S. GOVERNMENT PRINTING OFFICE :1973--542-650/73

(Continued from inside front cover)

NESC 51 Application of Meteorological Satellite Data in Analysis and Forecasting. Ralph K. Anderson, Jerome P. Ashman, Fred Bittner, Golden R. Farr, Edward W. Ferguson, Vincent J. Oliver, and Arthur H. Smith, September 1969. Price $1.75 (AD-697-033) Supplement price $0.65 (AD-740-017)

NESC 52 Data Reduction Processes for Spinning Flat-Plate Satellite-Borne Radiometers. Torrence H. MacDonald, July 1970. Price $0.50 (COM-71-00132)

NESC 53 Archiving and Climatological Applications of Meteorological Satellite Data. John A. Leese, Arthur L. Booth, and Frederick A. Godshall, July 1970. Price $1.25 (COM-71-00076)

NESC 54 Estimating Cloud Amount and Height From Satellite Infrared Radiation Data. P. Krishna Rao, July 1970. Price $0.25 (PB-194-685)

NESC 56 Time-Longitude Sections of Tropical Cloudiness (December 1966-November 1967). J. M. Wallace, July 1970. Price $0.50 (COM-71-00131)

NOAA Technical Reports

NESS 55 The Use of Satellite-Observed Cloud Patterns in Northern Hemisphere 500-mb Numerical Analysis. Roland E. Nagle and Christopher M. Hayden, April 1971. Price $0.55 (COM-73-50262)

NESS 57 Table of Scattering Function of Infrared Radiation for Water Clouds. Giichi Yamamoto, Masayuki Tanaka, and Shoji Asano, April 1971. Price $1.00 (COM-71-50312)

NESS 58 The Airborne ITPR Brassboard Experiment. W. L. Smith, D. T. Hilleary, E. C. Baldwin, W. Jacob, H. Jacobowitz, G. Nelson, S. Soules, and D. Q. Wark, March 1972. Price $1.25 (COM-72-10557)

NESS 59 Temperature Sounding From Satellites. S. Fritz, D. Q. Wark, H. E. Fleming, W. L. Smith, H. Jacobowitz, D. T. Hilleary, and J. C. Alishouse, July 1972. Price $0.55 (COM-72-50963)

NESS 60 Satellite Measurements of Aerosol Backscattered Radiation From the Nimbus F Earth Radiation Experiment. H. Jacobowitz, W. L. Smith, and A. J. Drummond, August 1972. Price $0.25 (COM-72-51031)

NESS 61 The Measurement of Atmospheric Transmittance From Sun and Sky With an Infrared Vertical Sounder. W. L. Smith and H. B. Howell, September 1972. Price $0.30 (COM-73-50020)

NESS 62 Proposed Calibration Target for the Visible Channel of a Satellite Radiometer. K. L. Coulson and H. Jacobowitz, October 1972. Price $0.35 (COM-73-10143)

NESS 63 Verification of Operational SIRS B Temperature Retrievals. Harold J. Brodrick and Christopher M. Hayden, December 1972. Price $0.55 (COM-73-50279)

NESS 64 Radiometric Techniques for Observing the Atmosphere From Aircraft. William L. Smith and Warren J. Jacob. January 1973. Price $0.35 (COM-73-50376)

NESS 65 Satellite Infrared Soundings From NOAA Spacecraft. L. M. McMillin, D. Q. Wark, J.M. Siomkajlo, P. G. Abel, A. Werbowetzki, L. A. Lauritson, J. A. Pritchard, D. S. Crosby, H. M. Woolf, R. C. Luebbe, M. P. Weinreb, H. E. Fleming, F. E. Bittner, and C. M. Hayden, September 1973.